

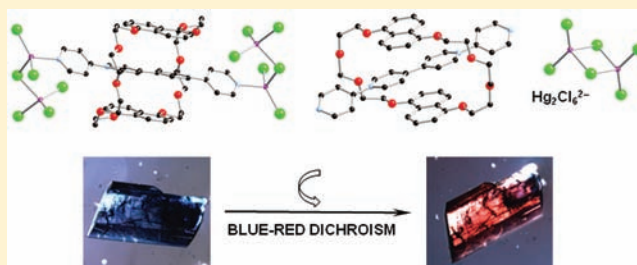
Blue-Colored, Linear Rigid-Axle [2]Pseudorotaxanes: Metal-Binding Properties, Crystal Structures, and Blue/Red Dichroism

Isurika R. Fernando and Gellert Mezei*

Department of Chemistry, Western Michigan University, Kalamazoo, Michigan 49008, United States

Supporting Information

ABSTRACT: Rare blue-colored [2]pseudorotaxanes based on the previously unexplored [*N,N'*-bis(4-pyridyl)-4,4'-bipyridinium]²⁺ axle and bis(1,5-naphtho)-32-crown-8 (BN32C8) or bis(1,5-naphtho)-38-crown-10 (BN38C10) wheels have been synthesized and characterized by UV-vis, ¹H NMR spectroscopy, and electrochemistry, and their metal-binding properties toward CdI₂ and HgCl₂ have been studied by optical absorption in solution and X-ray crystallography in the solid state. We report contrasting structures of the same metal and different wheels or the same wheel and different metals. We also show for the first time that a simple metal complex, such as Hg₂Cl₆²⁻, can induce a blue/red linear dichroism by organizing the [2]pseudorotaxane units into a columnar arrangement in the crystal.

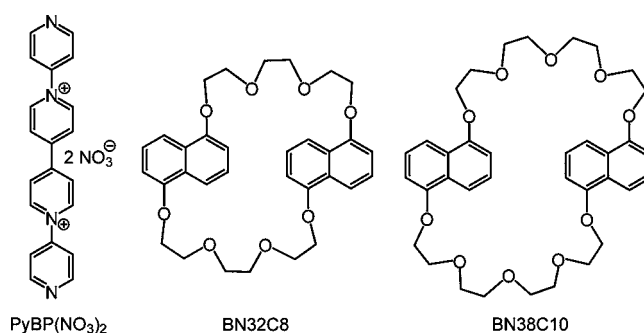


1. INTRODUCTION

Rotaxanes and pseudorotaxanes—supramolecules in which a wheel-like molecule can slide along or pirouette around a threaded axlelike molecule (bulky end groups prevent the wheel from dissociating in rotaxanes)—are some of the most important examples of materials that can be used for the construction of artificial molecular machines (AMMs).¹ The large number and variety of reported molecular analogues of different macroscopic devices suggests that these tiny machines might become the ultimate miniaturized components for future technologies.² As was recently pointed out by Grzybowski et al.,³ crystalline solid-state actuators and mechanized metal-organic frameworks (MOFs) based on organized assemblies of AMMs are some of the prime targets of nanofabrication. Despite the exponentially increasing amount of research in the field of molecular machines over the last 2 decades, a protocol for the assembly of rotaxanes into useful, ordered arrays is still lacking. A certain degree of organization has been achieved by building into liquid-crystalline phases⁴ and MOFs⁵ and by attachment to metal surfaces.⁶ Because the interaction of pseudorotaxanes with metal ions is not fully explored, we initiated a systematic study aiming at understanding and controlling the supramolecular/coordination chemistry of metal-rotaxane architectures.

We chose the 4,4'-bipyridinium/aromatic crown ether synthon for our studies (Scheme 1), for its color is a convenient, fast visual indicator of pseudorotaxane formation both in solution and in the solid state.⁷ In addition, the use of *rigid* and *linear* pseudorotaxanes is expected to lead to predictable and tunable rotaxane assemblies upon coordination to metal ions. The axle component used consists of *N,N'*-bis(4-pyridyl)-4,4'-bipyridinium (PyBP²⁺), while the wheel-compo-

Scheme 1. Pseudorotaxane Components Used in This Study



nent is either bis(1,5-naphtho)-32-crown-8 (BN32C8) or bis(1,5-naphtho)-38-crown-10 (BN38C10).

2. EXPERIMENTAL SECTION

2.1. Synthesis: General Remarks. All commercially available reagents were used as received. PyBP·[NO₃]₂,⁸ BN32C8,^{7a} and BN38C10⁹ were prepared according to reported procedures.

2.1.1. Synthesis of 1(CdI₂)-2CH₃OH (1 = PyBP/BN32C8). A solution of CdI₂ (4.2 mg, 11.5 mmol) in CH₃OH (1.5 mL) was layered over a solution of PyBP·[NO₃]₂ (2.5 mg, 5.7 mmol) and BN32C8 (2.7 mg, 5.1 mmol) in 1.5 mL of CH₃OH/CHCl₃ (1:1). After 2 weeks, the resulting clear solution was layered with ¹Pr₂O to obtain dark-blue X-ray-quality crystals.

2.1.2. Synthesis of 2-[CdI₄]-0.5CHCl₃-2CH₃OH (2 = PyBP/BN38C10). A solution of CdI₂ (4.2 mg, 11.4 mmol) in CH₃OH (1.5 mL) was layered over a solution of PyBP·[NO₃]₂ (2.5 mg, 5.7 mmol) and BN38C10 (3.2 mg, 5.1 mmol) in 1.5 mL of CH₃OH/CHCl₃

Received: December 6, 2011

Published: February 21, 2012

Table 1. Crystallographic Data

	1(CdI ₃) ₂ ·2CH ₃ OH	1·[Hg ₂ Cl ₆]	2·CdI ₄ ·0.5CHCl ₃ ·2CH ₃ OH	2(Hg ₂ Cl ₆) ₂ ·PyBP·2CH ₃ OH
formula	C ₅₄ H ₆₀ Cd ₂ I ₆ N ₄ O ₁₀	C ₅₂ H ₅₂ Cl ₆ Hg ₂ N ₄ O ₈ S	C _{58.5} H _{68.5} CdCl _{1.5} I ₄ N ₄ O ₁₂	C ₇₈ H ₈₄ Cl ₁₂ Hg ₄ N ₈ O ₁₂
fw	1911.26	1474.86	1692.85	2553.29
cryst syst	triclinic	triclinic	triclinic	triclinic
space group	P $\bar{1}$ (No. 2)	P $\bar{1}$ (No. 2)	P $\bar{1}$ (No. 2)	P $\bar{1}$ (No. 2)
a/Å	9.8786(2)	9.7025(2)	11.5238(4)	10.8869(1)
b/Å	16.8160(3)	11.5838(3)	13.9373(4)	14.7822(1)
c/Å	20.8803(3)	12.6269(3)	20.2886(7)	15.3243(1)
α /deg	98.642(1)	98.550(1)	86.472(2)	112.373(1)
β /deg	102.633(1)	103.965(1)	88.951(2)	100.917(1)
γ /deg	105.015(1)	101.351(1)	76.119(2)	103.572(1)
V/Å ³	3189.3(1)	1321.26(5)	3157.4(2)	2107.60(3)
Z	2	1	1	1
D _{calc} /g cm ⁻³	1.990	1.854	1.781	2.012
μ /mm ⁻¹	3.625	6.164	2.426	7.707
reflins collected/unique	102 629/18 525	57 649/7696	83 396/15 025	57 233/12 266
obsd reflns [$I > 2\sigma(I)$]	7402	6137	7194	7828
GO F (on F ²)	0.985	1.038	0.822	1.022
R(F), R _w (F) [$I > 2\sigma(I)$]	0.0730, 0.1363	0.0426, 0.0986	0.0859, 0.2105	0.0432, 0.0655

(1:1). Dark-orange-red X-ray-quality crystals were obtained after 7 weeks.

2.1.3. Synthesis of 1·[Hg₂Cl₆]. A solution of HgCl₂ (3.2 mg, 11.4 mmol) in CH₃OH (1.5 mL) was layered over a solution of PyBP·[NO₃]₂ (2.5 mg, 5.7 mmol) and BN32C8 (2.7 mg, 5.1 mmol) in 1.5 mL of CH₃OH/CHCl₃ (1:1). Dark-blue X-ray-quality crystals were obtained after 2 weeks.

2.1.4. Synthesis of 2(Hg₂Cl₆)₂·PyBP·2CH₃OH. A solution of HgCl₂ (3.2 mg, 11.4 mmol) in CH₃OH (1.5 mL) was layered over a solution of PyBP·[NO₃]₂ (2.5 mg, 5.7 mmol) and BN38C10 (3.2 mg, 5.1 mmol) in 1.5 mL of CH₃OH/CHCl₃ (1:1). Dark-blue X-ray-quality crystals were obtained after 2 weeks.

2.2. Instrumentation. NMR and UV–vis spectra were recorded at room temperature on Jeol JNM-ECP400 and Shimadzu UV 2101 PC spectrophotometers, respectively. Cyclic voltammetric measurements were performed using a Bioanalytical Systems (BAS) CV-50W electrochemical workstation. X-ray diffraction data were collected at 100 K from a single crystal mounted atop a glass fiber under Paratone-N oil with a Bruker SMART APEX II diffractometer using graphite-monochromated Mo K α ($\lambda = 0.710 73$ Å) radiation.

2.3.1. Experimental Procedures. *UV–Vis Spectroscopy.* Samples for UV–vis spectra were prepared in CH₃OH/CHCl₃ (1:1). Standard solutions of 1.000 (± 0.001) mM of the axle and wheel components, as well as the corresponding pseudorotaxanes, were prepared in 25.00 (± 0.01) mL volumetric flasks by using 10.910 (± 0.001), 13.715 (± 0.001), and 15.907 (± 0.001) mg of PyBP·[NO₃]₂, BN32C8, and BN38C10, respectively. Job's plot method with varying mole fractions of the axle and wheel was used to determine the stoichiometry of the pseudorotaxane complexes. Solutions of the axle and wheel components were mixed using a micropipet to obtain the different axle–wheel ratios in a final volume of 3.00 (± 0.01) mL (Table S1 in the Supporting Information). The absorption maxima at 0.5 mole fraction indicate a 1:1 stoichiometry for both pseudorotaxanes (Figure S1 in the Supporting Information). Benesi–Hildebrand analysis was used to determine the equilibrium association constants of the 1:1 pseudorotaxanes (Figure S2 in the Supporting Information). A 0.500 (± 0.005) mM standard solution of the axle was prepared in a 10.00 (± 0.01) mL volumetric flask by dissolving 2.182 (± 0.001) mg of PyBP·[NO₃]₂ in CH₃OH/CHCl₃ (1:1). A standard solution of the pseudorotaxane was prepared by dissolving 6.858 (± 0.001) mg of BN32C8 or 7.953 (± 0.001) mg of BN38C10 in 2.50 mL of a PyBP·[NO₃]₂ standard solution. A volume of 2.00 (± 0.01) mL of the standard axle

solution was transferred into a cuvette and titrated with the pseudorotaxane solution up to a wheel/axle ratio of 5:1.

2.3.2. NMR Spectroscopy. Solutions of 3.822 (± 0.006) mM of the axle and wheel components were prepared by dissolving 1.000 (± 0.001) mg of PyBP·[NO₃]₂, 1.258 (± 0.001) mg of BN32C8, and 1.258 (± 0.001) mg of BN38C10, respectively, in 600 (± 1) μ L of CD₃OD/CDCl₃ (1:1). Solutions of 3.822 (± 0.006) mM of pseudorotaxanes 1·[NO₃]₂ and 2·[NO₃]₂ were prepared by mixing 1.000 (± 0.001) mg of PyBP·[NO₃]₂ and either 1.258 (± 0.001) mg of BN32C8 or 1.258 (± 0.001) mg of BN38C10 in 600 (± 1) μ L of CD₃OD/CDCl₃ (1:1). The proton assignments for the spectra (Figures S3 and S4 in the Supporting Information) are shown in Scheme S1 in the Supporting Information.

2.3.3. Cyclic Voltammetry. The composite electrode system, containing platinum wires (0.4 mm) as working and counter electrodes and silver wire as a quasi-reference electrode, was polished with a 0.05 μ m Al₂O₃/water slurry on a flat surface. Tetrabutylammonium hexafluorophosphate (Bu₄NPF₆, 0.1 M) was used as the supporting electrolyte and ferrocene (Fc) as the internal standard. The sample solutions were purged with purified nitrogen and kept under an inert atmosphere throughout the measurements. Potentials are reported versus Fc/Fc⁺. A 0.5 mM solution of PyBP(PF₆)₂ was prepared in a 5.00 mL volumetric flask by dissolving 3.010 (± 0.001) mg of PyBP(PF₆)₂ in a CH₃CN/CH₂Cl₂ (2:1) mixture. A 0.5 mM PyBP(PF₆)₂/BN38C10 pseudorotaxane solution was prepared in a 5.00 mL volumetric flask by dissolving 3.010 (± 0.001) mg of PyBP(PF₆)₂ and 3.181 (± 0.001) mg of BN38C10 in a CH₃CN/CH₂Cl₂ (2:1) mixture. A 0.5 mM PyBP(PF₆)₂/BN32C8 pseudorotaxane solution was prepared similarly, using 2.743 (± 0.001) mg of BN32C8.

2.3.4. X-ray Crystallography. Once removed from the mother liquor, solvent-containing rotaxane crystals are sensitive to solvent loss at ambient conditions and were mounted quickly under the cryostream to prevent decomposition. The structures were solved by employing the direct methods program *SHELXTL* and refined by full-matrix least squares on F², using the *APEX2 v2008.2-0* software package.¹⁰ All non-H atoms were refined with independent anisotropic displacement parameters, except the disordered crown ether molecule in 2·CdI₄·0.5CHCl₃·2CH₃OH and the disordered methanol (MeOH) solvent molecule in 2(Hg₂Cl₆)₂·PyBP·2CH₃OH. Crystallographic details are summarized in Table 1, and packing diagrams are shown in Figures S5–S8 in the Supporting Information. One of the two crystallographically independent crown ether molecules in 2·CdI₄·0.5CHCl₃·2CH₃OH is severely disordered. The whole-molecule disorder was modeled over two positions (Figure S9 in the Supporting Information). Some residual electron density around the

disordered crown ether molecule suggests that the latter is possibly disordered over more than two positions. Within the same structure, the I3 and I4 atoms are disordered over two positions, and two of the three MeOH solvent molecules are disordered with a chloroform molecule (50:50 occupancy).

3. RESULTS AND DISCUSSION

A mixture of the axle (yellow PyBP^{2+} nitrate salt) and wheel (colorless crown ether) in $\text{MeOH}/\text{CHCl}_3$ (2:1) displays a deep-blue color with absorption maxima at 607 and 588 nm in the case of BN32C8 and BN38C10, respectively (Figure 1).

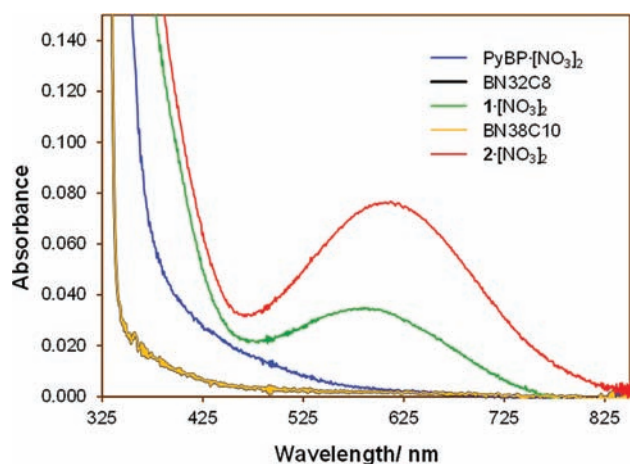


Figure 1. UV-vis spectra of 1 mM solutions of $\text{PyBP}\cdot[\text{NO}_3]_2$, BN32C8, BN38C10, $1\cdot[\text{NO}_3]_2$, and $2\cdot[\text{NO}_3]_2$ in $\text{CH}_3\text{OH}/\text{CHCl}_3$ (1:1).

This is a surprising result because the 4,4'-bipyridinium/bis(1,5-naphtho) chromophore is known to display a red/orange color.^{7,11} Indeed, analogous [2]pseudorotaxanes with (carboethoxy)propyl instead of pyridyl groups display absorption maxima at 501 and 490 nm, respectively.^{7a} The color of these pseudorotaxanes is due to charge transfer from the highest occupied molecular orbital (HOMO) of the π -electron-rich aromatic crown ether wheel to the lowest unoccupied molecular orbital (LUMO) of the π -electron-poor bipyridinium axle. The drastic color difference is attributed to a decrease in the LUMO energy level of the axle on going from the σ -donor (carboethoxy)propyl substituent to the π -acceptor pyridyl substituent, leading to a reduction of the HOMO–LUMO energy gap of the (pseudo)rotaxane. This is in accord with preliminary electrochemical measurements, which show a large shift of the axle's two reduction potentials from -0.76 and -1.20 V^{7a} to -0.51 and -0.75 V (Figure 2). A similar effect was observed in the only other blue rotaxane known, where fluorination led to an increase of the HOMO energy level of the π -donor axle, resulting in a reduction of the HOMO–LUMO energy gap.¹²

Job's plots obtained by optical absorption measurements indicate 1:1 complexation stoichiometries in solution (Figure S1 in the Supporting Information), while a Benesi–Hildebrand analysis provides association constants of $8.70 (\pm 0.70) \times 10^2$ and $4.20 (\pm 0.20) \times 10^2 \text{ M}^{-1}$ for $[\text{PyBP}/\text{BN32C8}][\text{NO}_3]_2$ ($1\cdot[\text{NO}_3]_2$) and $[\text{PyBP}/\text{BN38C10}][\text{NO}_3]_2$ ($2\cdot[\text{NO}_3]_2$), respectively (Figure S2 in the Supporting Information). Significant shifts in the ^1H NMR spectra in $\text{CD}_3\text{OD}/\text{CDCl}_3$ (2:1) relative to the free components confirm complex formation in solution (Figures S3 and S4 in the Supporting

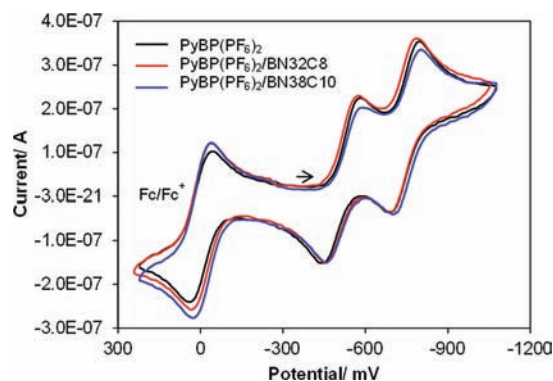


Figure 2. Cyclic voltammetry traces.

Information). The absence of a new set of peaks upon the addition of excess axle or wheel components to a 1:1 mixture indicates a fast exchange equilibrium between the pseudorotaxane and its individual components at room temperature. A decrease in the intensity of the color with increasing temperature is indicative of an entropy-driven, temperature-dependent equilibrium between the colored pseudorotaxane and colorless axle/wheel components.^{7a}

The addition of CdI_2 in a 1:1 ratio to a solution of $1\cdot[\text{NO}_3]_2$ in $\text{MeOH}/\text{CHCl}_3$ (1:1) causes an increase in the absorption intensity of the charge-transfer band in the UV-vis spectrum, with virtually no shift of the absorption maximum (Figure 3).

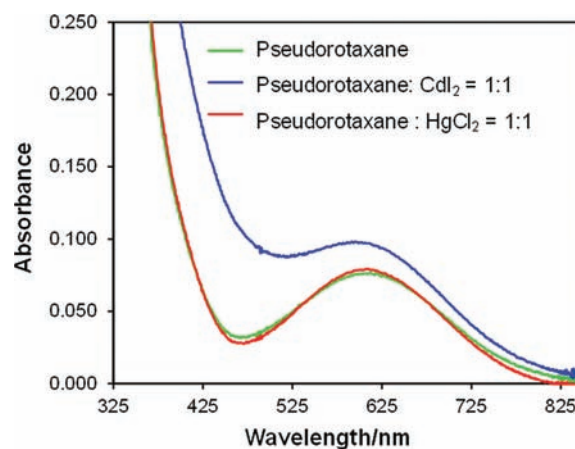


Figure 3. UV-vis spectra of the $[\text{PyBP}/\text{BN32C8}][\text{NO}_3]_2$ pseudorotaxane with CdI_2 and HgCl_2 in a $\text{CH}_3\text{OH}/\text{CHCl}_3$ (1:1) solution.

The increased absorbance is an indication of metal binding in solution. The addition of CdI_2 in 2:1 or higher ratios to the [2]pseudorotaxane solution leads to precipitation. In contrast, the addition of HgCl_2 in a 1:1, 2:1, or 3:1 ratio does not produce any significant changes, indicating no metal binding (Figure S10 in the Supporting Information). Similar results were obtained with $2\cdot[\text{NO}_3]_2$ (Figure S11 in the Supporting Information).

Upon standing, single crystals suitable for X-ray diffraction were obtained from the above solutions in all four cases (dark blue, with the exception of $2\cdot[\text{CdI}_4]\cdot\text{CHCl}_3\cdot\text{CH}_3\text{OH}$, dark orange-red; $1\cdot[\text{Hg}_2\text{Cl}_6]$ appears blue or red as viewed from different directions). The neutral cadmium and mercury dihalides were converted into anionic CdI_3^- , CdI_4^{2-} , and $\text{Hg}_2\text{Cl}_6^{2-}$ in solution and produced discrete instead of extended structures, despite the ditopic nature of the pseudorotaxane

ligands. A similar phenomenon of in situ anionic metal halide formation was observed in the case of CoBr_2 and MnBr_2 with a different pseudorotaxane, although in that case, the extra Br^- ions were not acquired by anion scrambling but were available as the counterion of the axle.¹³ The CdI_3^- anions formed from CdI_2 in the presence of **1** bind to both ends of the pseudorotaxane unit, leading to a dizwitterionic [2]rotaxane (Figures 4 and S5 in the Supporting Information). In the case

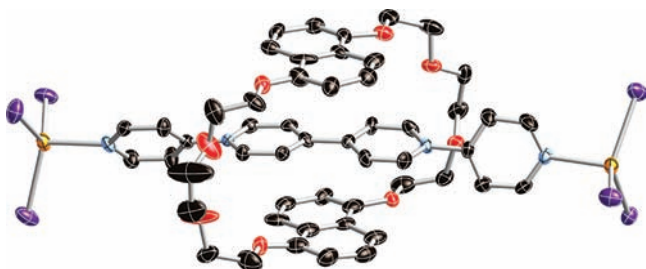


Figure 4. Thermal ellipsoid plot (30%) of $1(\text{CdI}_3)_2 \cdot 2\text{CH}_3\text{OH}$. H atoms and solvent molecules are omitted for clarity. Color code: Cd, orange; I, violet; O, red; N, blue; C, black.

of **2**, the CdI_4^{2-} anion is formed, which does not bind to the pseudorotaxane but acts as a counterion (Figures 5 and S6 in

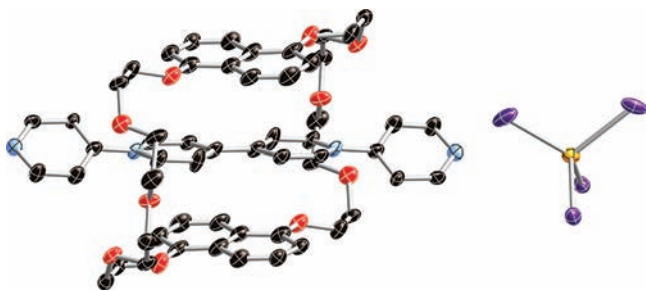


Figure 5. Thermal ellipsoid plot (30%) of $2 \cdot [\text{CdI}_4] \cdot \text{CHCl}_3 \cdot \text{CH}_3\text{OH}$. Only one of the two crystallographically independent pseudorotaxane units is shown. H atoms and solvent molecules are omitted for clarity.

the Supporting Information). In contrast, the $\text{Hg}_2\text{Cl}_6^{2-}$ anion generated from Hg_2Cl_2 has an opposite binding pattern: it does not bind to pseudorotaxane **1** (Figures 6 and S7 in the Supporting Information) but forms a [2]rotaxane with **2** (Figures 7 and S8 in the Supporting Information).

The [2](pseudo)rotaxane units sit on inversion centers except in $1(\text{CdI}_3)_2$. In all four cases, the bipyridinium core (PyBP^{2+}) is symmetrically located between the two naphthalene units of the crown ether at distances of 3.23(1), 3.42(1), 3.24(1), and 3.39(1) Å, respectively. The considerably shorter π - π -stacking distances observed in the BN32C8 [2](pseudo)rotaxanes (3.23–3.24 Å) than in the BN38C10 ones (3.39–3.42 Å) are consistent with the twice larger binding strength of BN32C8 to PyBP^{2+} vs BN38C10 measured in solution. Multiple C–H \cdots O hydrogen bonds between the axle and wheel components ranging from 2.22(1) to 2.51(1) Å are observed. The terminal N–N distances in the bipyridinium axles are 15.38(1), 15.49(1), 15.49(1), and 15.42(1) Å, respectively, indicating a rather constant length of the [2](pseudo)rotaxane struts in the four compounds studied. The two pyridine units of the bipyridinium core are coplanar in all cases except in $1(\text{CdI}_3)_2$, in which they are at a 6.2° angle. The two terminal pyridine units are rotated at 35.4, 31.0, and

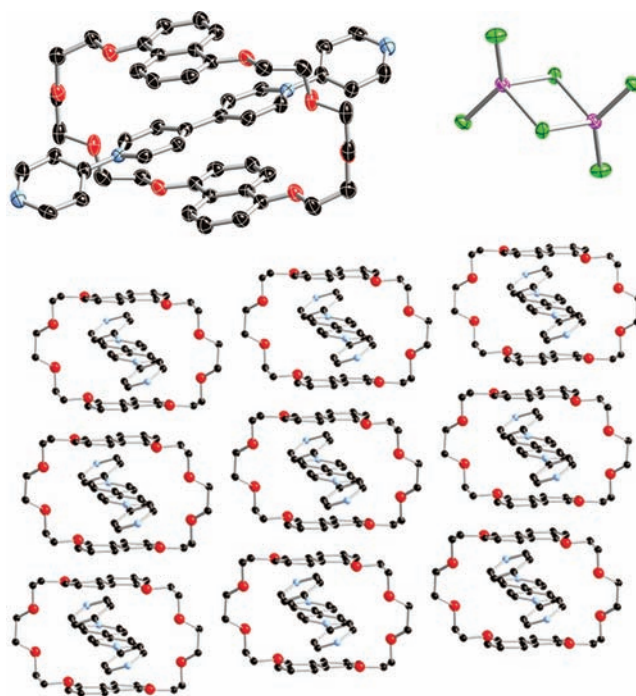


Figure 6. Thermal ellipsoid plot (50%) of $1 \cdot [\text{Hg}_2\text{Cl}_6]$. Top: Molecular structure. Bottom: Packing diagram showing the columnar arrangement of pseudorotaxane units (H atoms and $\text{Hg}_2\text{Cl}_6^{2-}$ counterions are omitted for clarity). Color code: Hg, purple; Cl, green; O, red; N, blue; C, black.



Figure 7. Thermal ellipsoid plot (50%) of $2(\text{Hg}_2\text{Cl}_6)_2 \cdot \text{PyBP} \cdot 2\text{CH}_3\text{OH}$. The free PyBP^{2+} , H atoms, and solvent molecules are omitted for clarity.

38.0° to the same side of the BP^{2+} core in the case of $2 \cdot [\text{CdI}_4]$, $1 \cdot [\text{Hg}_2\text{Cl}_6]$, and $2(\text{Hg}_2\text{Cl}_6)_2 \cdot \text{PyBP}$, while they are rotated at 51.1 and 66.9° to opposite sides of the BP^{2+} core in $1(\text{CdI}_3)_2$. An additional PyBP^{2+} molecule is found in the structure of $2(\text{Hg}_2\text{Cl}_6)_2$ as a counterion.

In all four structures, the metal ions are found in distorted tetrahedral coordination environments. The Cd–N bond lengths of 2.320(7) and 2.345(7) Å lie within the 2.266–2.421 Å range for Cd–N distances found in complexes reported in the Cambridge Structural Database (CSD) containing the PyCdI_3 unit. The Hg–N bond length of 2.317(4) Å also lies within the 2.113–2.445 Å range found in other reported PyHgCl_3 -containing complexes. While there are 44 compounds reported in the CSD containing the discrete $[\text{Hg}_2\text{Cl}_6]^{2-}$ unit, $2(\text{Hg}_2\text{Cl}_6)_2 \cdot \text{PyBP}$ is the first example where this metal complex binds to an N-donor ligand. It is important to note that the particular metal halide structures found in these (pseudo)rotaxane crystals are not specific to either the respective metal or the halide. A plethora of $\text{M}_a\text{X}_b^{n-}$ complexes

(M = Cd or Hg; X = Cl or I), obtained under various different conditions, are found in the CSD. It is therefore reasonable to conclude that the CdI_3^- , CdI_4^{2-} , and $\text{Hg}_2\text{Cl}_6^{2-}$ complexes found in our structures were selectively incorporated from a mixture of $\text{M}_a\text{X}_b^{n-}$ species present in solution during crystal growth, to provide the most stable crystal lattice in each particular case.

Optical absorption micrographs of $1 \cdot [\text{Hg}_2\text{Cl}_6]$ taken under polarized light show that the crystal drastically changes color from blue to red (and vice versa) upon rotation around the perpendicular axis (Figure 8). A closer examination of the

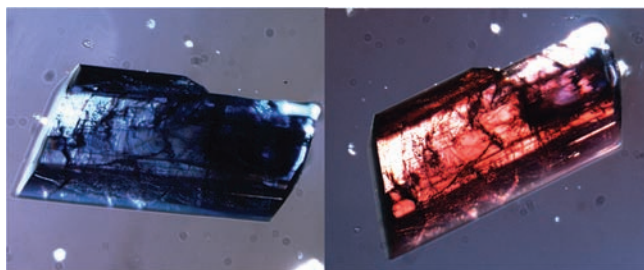


Figure 8. Optical micrographs of the same crystal of $1 \cdot [\text{Hg}_2\text{Cl}_6]$ in two different orientations (under Paratone-N oil).

packing diagram reveals a columnar arrangement of the pseudorotaxane units and points to the large observed anisotropy (Figure 6). A similar blue/red linear dichroic emission from a triarylmethane dye has recently been reported.¹⁴ We are currently working on the detailed spectroscopic characterization of this unusual structure, aiming at possible applications in optoelectronics.

4. CONCLUSIONS

In summary, we showed that a previously unexplored pyridine-substituted axle molecule leads to a rare blue [2]-pseudorotaxane motif and that a subtle difference in the size of the wheel component has a critical role in the binding of the pseudorotaxane to a particular metal complex. We also observed widely different binding affinities of the same pseudorotaxane unit to different metal halide complexes, resulting in crystals with surprising dichroic behavior. A systematic study of metal–rotaxane complexes involving differently charged axle and wheel components, as well as a variety of metal complexes, is underway.

■ ASSOCIATED CONTENT

Supporting Information

Details of pseudorotaxane stoichiometry, association constant, and extinction coefficient determinations, NMR spectra, metal binding, and crystallographic details in CIF format. This material is available free of charge via the Internet at <http://pubs.acs.org>.

■ AUTHOR INFORMATION

Corresponding Author

*E-mail: gellert.mezei@wmich.edu.

Notes

The authors declare no competing financial interest.

■ ACKNOWLEDGMENTS

We thank Western Michigan University for funding (Support for Faculty Scholars Award).

■ REFERENCES

- (1) (a) Sauvage, J. P.; Dietrich-Buchecker, C., Eds. *Molecular Catenanes, Rotaxanes, and Knots*; Wiley-VCH: Weinheim Germany, 1999. (b) Amabilino, D. B.; Stoddart, J. F. *Chem. Rev.* **1995**, *95*, 2725. (c) Blanco, M.-J.; Jimenez, M. C.; Chambron, J.-C.; Heitz, V.; Linke, M.; Sauvage, J.-P. *Chem. Soc. Rev.* **1999**, *28*, 293. (d) Huang, F.; Gibson, H. W. *Prog. Polym. Sci.* **2005**, *30*, 982. (e) Wenz, G.; Han, B.-H.; Müller, A. *Chem. Rev.* **2006**, *106*, 782. (f) Crowley, J. D.; Goldup, S. M.; Lee, A.-L.; Leigh, D. A.; McBurney, R. T. *Chem. Soc. Rev.* **2009**, *38*, 1530.
- (2) (a) Boyle, M. M.; Smaldone, R. A.; Whalley, A. C.; Ambrogio, M. W.; Botros, Y. Y.; Stoddart, J. F. *Chem. Sci.* **2011**, *2*, 204. (b) Sauvage, J. P., Gaspard, P., Eds. *From Non-Covalent Assemblies to Molecular Machines*; Wiley-VCH: Weinheim, Germany, 2010. (c) Stoddart, J. F. *Chem. Soc. Rev.* **2009**, *38*, 1802. (d) Balzani, V.; Credi, A.; Venturi, M. *Molecular Devices and Machines—Concepts and Perspectives for the Nanoworld*; Wiley-VCH: Weinheim, Germany, 2008. (e) Balzani, V.; Credi, A.; Raymo, F. M.; Stoddart, J. F. *Angew. Chem., Int. Ed.* **2000**, *39*, 3348.
- (3) Coskun, A.; Banaszak, M.; Astumian, R. D.; Stoddart, J. F.; Grzybowski, B. A. *Chem. Soc. Rev.* **2012**, *41*, 19.
- (4) (a) Yasuda, T.; Tanabe, K.; Tsuji, T.; Coti, K. K.; Aprahamian, I.; Stoddart, J. F.; Kato, T. *Chem. Commun.* **2010**, *46*, 1224. (b) Kidowaki, M.; Nakajima, T.; Araki, J.; Inomata, A.; Ishibashi, H.; Ito, K. *Macromolecules* **2007**, *40*, 6859.
- (5) (a) Kim, K. *Chem. Soc. Rev.* **2002**, *31*, 96. (b) Loeb, S. J. *Chem. Soc. Rev.* **2007**, *36*, 226. (c) Li, Q.; Zhang, W.; Miljanić, O. Š.; Sue, C.-H.; Knobler, C.; Zhao, Y.-L.; Liu, L.; Stoddart, J. F.; Yaghi, O. M. *Science* **2009**, *325*, 855.
- (6) (a) Davis, J. J.; Orłowski, G. A.; Rahman, H.; Beer, P. D. *Chem. Commun.* **2010**, *46*, 54. (b) Credi, A.; Silvi, S.; Venturi, M. In *The Supramolecular Chemistry of Organic-Inorganic Hybrid Materials*; Rurack, K., Martínez-Máñez, Eds.; John Wiley & Sons, Inc.: New York, 2010; p 503.
- (7) (a) Fernando, I. R.; Bairu, S. G.; Ramakrishna, G.; Mezei, G. *New J. Chem.* **2010**, *34*, 2097. (b) Mezei, G.; Kampf, J. W.; Pecoraro, V. L. *New J. Chem.* **2007**, *31*, 439.
- (8) Reuss, R. H.; Winters, L. J. *J. Org. Chem.* **1973**, *38*, 3993.
- (9) Hamilton, D. G.; Davies, J. E.; Prodi, L.; Sanders, J. K. M. *Chem.—Eur. J.* **1998**, *4*, 608.
- (10) APEX2 v2008.2-0; Bruker AXS Inc.: Madison, WI, 2008.
- (11) (a) Ashton, P. R.; Chrystal, E. J. T.; Mathias, J. P.; Parry, K. P.; Slawin, A. M. Z.; Spencer, N.; Stoddart, J. F.; Williams, D. J. *Tetrahedron Lett.* **1987**, *28*, 6367. (b) Ortholand, J.-Y.; Slawin, A. M. Z.; Spencer, N.; Stoddart, J. F.; Williams, D. J. *Angew. Chem., Int. Ed. Engl.* **1989**, *28*, 1394. (c) Amabilino, D. B.; Ashton, P. R.; Balzani, V.; Boyd, S. E.; Credi, A.; Lee, J. Y.; Menzer, S.; Stoddart, J. F.; Venturi, M.; Williams, D. J. *J. Am. Chem. Soc.* **1998**, *120*, 4295. (d) Cabezon, B.; Cao, J.; Raymo, F. M.; Stoddart, J. F.; White, A. J. P.; Williams, D. J. *Chem.—Eur. J.* **2000**, *6*, 2262.
- (12) Ikeda, T.; Aprahamian, I.; Stoddart, J. F. *Org. Lett.* **2007**, *9*, 1481.
- (13) Davidson, G. J. E.; Loeb, S. J.; Parekh, N. A.; Wisner, J. A. J. *Chem. Soc., Dalton Trans.* **2001**, 3135.
- (14) Houjou, H.; Takezawa, S.; Oyamada, I.; Matsumura, K.; Seino, H.; Yoshikawa, I.; Mizobe, Y.; Araki, K. *Chem.—Eur. J.* **2011**, *17*, 1122.